

# The light pollution as a surrogate for urban population of the US cities

Felipe G. Operti<sup>1</sup>, Erneson A. Oliveira<sup>1,2</sup>, Humberto A. Carmona<sup>1</sup>, Javam C. Machado<sup>3</sup>, José S. Andrade Jr.<sup>1</sup>

<sup>1</sup> *Departamento de Física, Universidade Federal do Ceará, Fortaleza, Ceará, Brasil*

<sup>2</sup> *Programa de Pós-Graduação em Informática Aplicada, Universidade de Fortaleza, Fortaleza, Ceará, Brasil*

<sup>3</sup> *Departamento de Computação, Universidade Federal do Ceará, Fortaleza, Ceará, Brasil*

(Dated: June 19, 2017)

## Abstract

We show that the definition of the city boundaries can have a dramatic influence on the scaling behavior of the night-time light (NTL) as a function of population (POP) in the US. Precisely, our results show that the arbitrary geopolitical definition based on the Metropolitan/Consolidated Metropolitan Statistical Areas (MSA/CMSA) leads to a sublinear power-law growth of NTL with POP. On the other hand, when cities are defined according to a more natural agglomeration criteria, namely, the City Clustering Algorithm (CCA), an isometric relation emerges between NTL and population. This discrepancy is compatible with results from previous works showing that the scaling behaviors of various urban indicators with population can be substantially different for distinct definitions of city boundaries. Moreover, considering the CCA definition as more adequate than the MSA/CMSA one because the former does not violate the expected extensivity between land population and area of their generated clusters, we conclude that, without loss of generality, the CCA measures of light pollution and population could be interchangeably utilized in future studies.

## Introduction

More than 80% of the world and more than 90% of the US and European populations live under light-polluted skies (exposition to light at night) [1]. Since the first electric-powered illumination in the second half of the 19th century, the world has become covered by artificial electric light, changing drastically the night view of the Earth from space. The spreading of artificial electric light plays an important role on the duration of the *productive day*, not only for working but also for recreational activities. If in one hand the benefits of artificial light are quite evident, on the other hand, scientific researches suggest that the exposition to light at night could have adverse effects on both human and wildlife health [2–9]. For example, in humans, the pineal and blood melatonin rhythms are quickly disturbed by light pollution. Such studies argue that the night light exposure have two major physiological effects: they disrupt the circadian rhythms and suppress the production of melatonin [8]. This repeated suppression may have large consequences for the mammals health. For instance, it was shown that the suppression of the melatonin at night accelerates the metabolic activity and growth of rat hepatoma [5] and human breast cancer [3]. Moreover, the disruption of circadian rhythms made by the exposure of light at night might plays a crucial role in the etiology of depression [8].

The significant consequences of the exposure to night-time light (NTL) with the fact that 54% of world's population lives in urban areas stimulates the interest in understanding how the light pollution evolves with the size of the US cities [10]. Bettencourt *et al.* found the cities in the US exhibit three different types of allometric laws for urban indicators with population size [11]: (i) *Superlinear*. The superlinear urban indicators increase proportionally more than the population of the cities. Such behavior is intrinsically associated with the *social currency* of a city, indicating that larger cities are associated with optimal levels of human productivity and quality of life. Doubling the city size leads to a larger-than-double increment in productivity and life standards [11–13]. For example, wages, income, growth domestic product (GDP), bank deposits, as well as rates of invention measured by the number of patents and employment in creative sectors show a superlinear behavior [11]. (ii) *Linear* or *isometric relation*. The increasing of the linear urban indicators is proportional to the increasing of the population reflecting the common individual human needs, like the number of jobs, houses, and water consumption [11]. (iii) *Sublinear*. The sublinear urban indicators increase proportionally less than the population of the cities. This case is a manifestation of the *economy of scale*. The sublinearity is found in the number of gasoline stations, length of electrical cables, and road surfaces (material and infrastructure) cases [11].

From the results shown by Bettencourt *et al.*, several studies have been carried out on the allometry of urban indicators in different levels of human aggregation [14–17]. Following this aim, we analyze and classify the allometric law between the NTL and the population of the US cities.

Here, we use three geo-referenced dataset: the population dataset, the NTL dataset and the Metropolitan/Consolidated Metropolitan Statistical Area (MSA/CMSA). In order to define the boundaries of each US city, we use two methods: the City Clustering Algorithm (CCA) [18–20] and the MSA/CMSA [21]. Finally, we find the allometric scaling between the NTL and the population for the two applied methods. Furthermore, to compare them, we analyze the allometric scaling between area and population.

## Materials and Method

### Population dataset (GPWv4)

The population dataset is extracted from the fourth version of the Gridded Population of the World (GPWv4) [22, 23] from the Center for International Earth Science Information Network (CIESIN) at the Columbia University. The GPWv4 models the human population distribution on a continuous surface at high resolution. Population input data is collected through several censuses around the US, between 2005 and 2014. Data are provided in grid form, where each cell is formed by 30 arc-second angles (approximately  $1 \text{ km} \times 1 \text{ km}$  at the Equator line). We use the US population count data, measured in number of people, for the year 2015, as depicted in Fig. 1a.

The method successively introduced requires the population density of each grid cell. Therefore, we calculated the area of each grid cell dividing them into two spherical triangles. The area of a spherical triangle with edges  $a$ ,  $b$  and  $c$  is given by,

$$A = R^2 E, \quad (1)$$

where  $R = 6,378.137 \text{ km}$  is the Earth's radius and the spherical excess  $E$  is defined by the following expression:

$$E = 4 \tan^{-1} \left[ \tan \left( \frac{s}{2} \right) \tan \left( \frac{s_a}{2} \right) \tan \left( \frac{s_b}{2} \right) \tan \left( \frac{s_c}{2} \right) \right]^{1/2}. \quad (2)$$

with  $s = (a/R + b/R + c/R)/2$ ,  $s_a = s - a/R$ ,  $s_b = s - b/R$ , and  $s_c = s - c/R$ . In this context, the distance between two points,  $i$  and  $j$ , on the Earth's surface is calculated by,

$$d_{ij} = R\theta, \quad (3)$$

with

$$\theta = \cos^{-1} [\sin(y_i) \sin(y_j) + \cos(y_i) \cos(y_j) \cos(x_j - x_i)]. \quad (4)$$

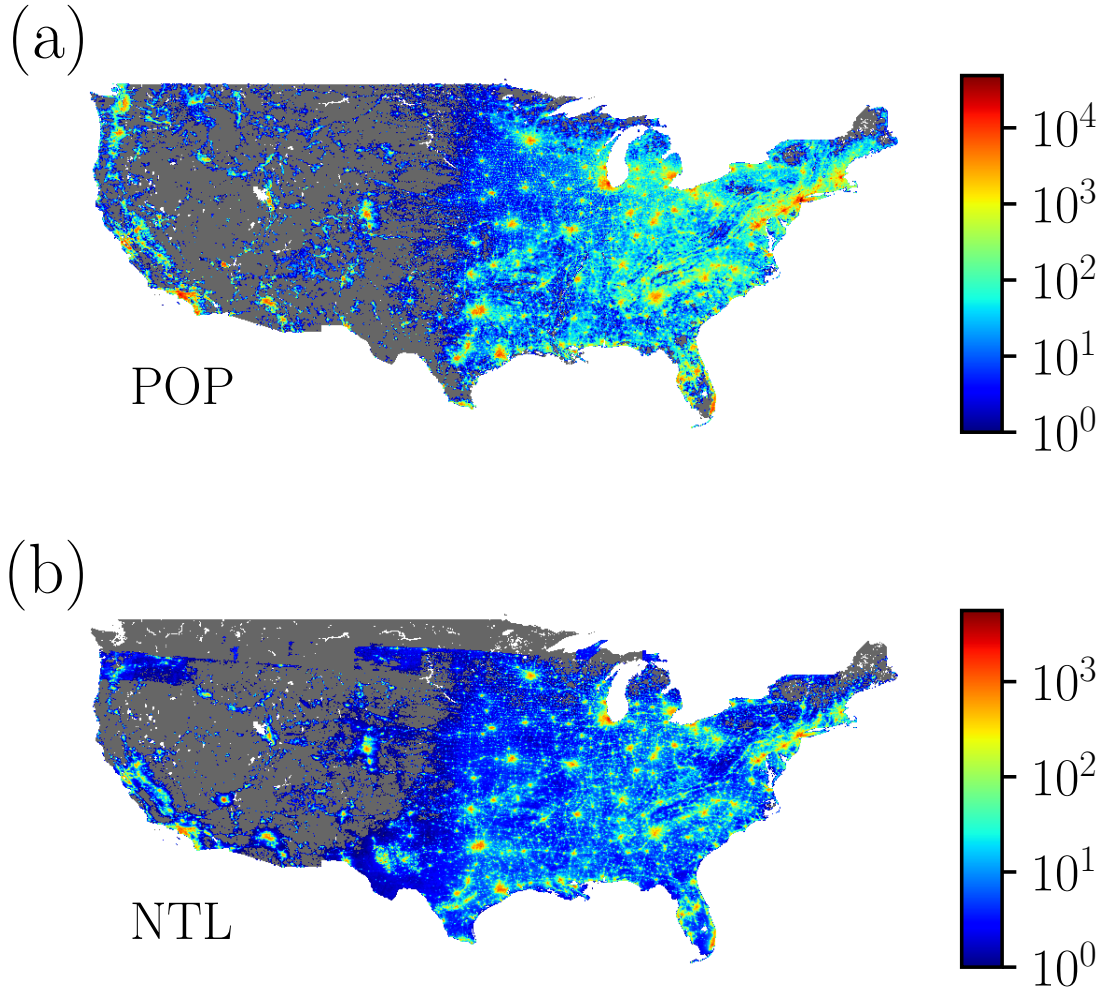


FIG. 1. **Datasets (on colors).** (a) The population dataset is defined as a 30 arc-second geolocated grid. It is obtained from the GPWv4 in logarithmic scale for the year 2015 [22, 23]. (b) The NTL dataset is obtained through the night-time light radiance emission data from the VIIRS DNB in  $nW/cm^2/sr$  [24–26]. It is defined at the resolution of 15 arc-second grid in logarithmic scale for the year 2015 (April).

In this formalism, the values of  $x_i$  ( $x_j$ ) and  $y_i$  ( $y_j$ ) are the longitude and latitude, respectively, of the point  $i$  ( $j$ ), measured in radians.

#### **Night-time light dataset (NTL)**

The NTL dataset is given by the night-time light radiance emission data from the National Centers for Environmental Information (NCEI) [25]. The NTL dataset is defined by the monthly average of radiance, measured in  $nW/cm^2/sr$ , using the night-time data from the scanning radiometer Visible Infrared Imaging Radiometer Suite (VIIRS) Day/Night Band (DNB) [24–26]. The VIIRS DNB data are processed and filtered in order to exclude data impacted by the lunar

illumination, lightning and cloud-cover, but they are susceptible to other temporal lights, *e.g.* aurora, fires, and boats [24, 25]. Such data span through the entire globe with a resolution of 15 arc-second (approximately  $500\text{ m} \times 500\text{ m}$  at the Equator line) between the latitudes  $75^\circ$  North and  $65^\circ$  South. We use the US data for the year 2015 (April), as shown in Fig. 1b.

### **Metropolitan Statistical Area (MSA), Primary Metropolitan Statistical Area (PMSA) and Consolidated Metropolitan Statistical Area (CMSA)**

The MSA are geographic entities with high degree of socioeconomic integration and population over 50,000 people. The PMSA are quite similar to MSA, however they present population over 1,000,000 people. The CMSA are metropolitan regions defined by the agglomeration of some PMSA. They are all delineated by the Office of Management and Budget (OMB) and provided by the US Census Bureau [21].

### **Data processing**

In order to superimpose the datasets, we perform two processes: (i) As the NTL grid has a higher resolution than the GPWv4 grid, we sum the values of all NTL grid cells, which their geolocated centers are within the same geolocated GPWv4 grid cell. Therefore, we produce a new NTL grid with the same positioning and resolution of the GPWv4 dataset; (ii) For the MSA/CMSA case, we use the same approach of (i), even though the MSA/CMSA are complex polygons. To deal with this problem, we use the even-odd rule algorithm [27]. Thus, we define the NTL value for each MSA/CMSA.

### **City Clustering Algorithm (CCA)**

We define the boundaries of each US city by applying the CCA to the population grid [18–20]. We use the continuum CCA that depends on two parameters, namely, a population density threshold,  $D^*$  and a cutoff length,  $\ell$  [20]. For the  $i$ -th grid cell, the population density  $D_i$  is georeferenced in its geometric center (shown as small black circles in Fig. 2). If  $D_i > D^*$ , the  $i$ -th grid cell is populated. In Fig. 2 the populated cells are shown in grey and red. Next, the algorithm selects a populated cell (red cell in Fig. 2a) and aggregates in the same cluster all nearest populated cells which are within a distance  $\ell$  from each (red cells in Figs. 2b, 2c and 2d). The Fig. 2 shows the four steps to determine the red cluster.

## **Results**

We apply the CCA to the population grid varying  $D^*$  (in  $people/km^2$ ), from 0 to 10000, and  $\ell$  (in  $km$ ), from 1 to 20. For all pairs of parameters, we find that it is possible to statistically correlate through power-law relations the area and the population as well as the NTL and the population of

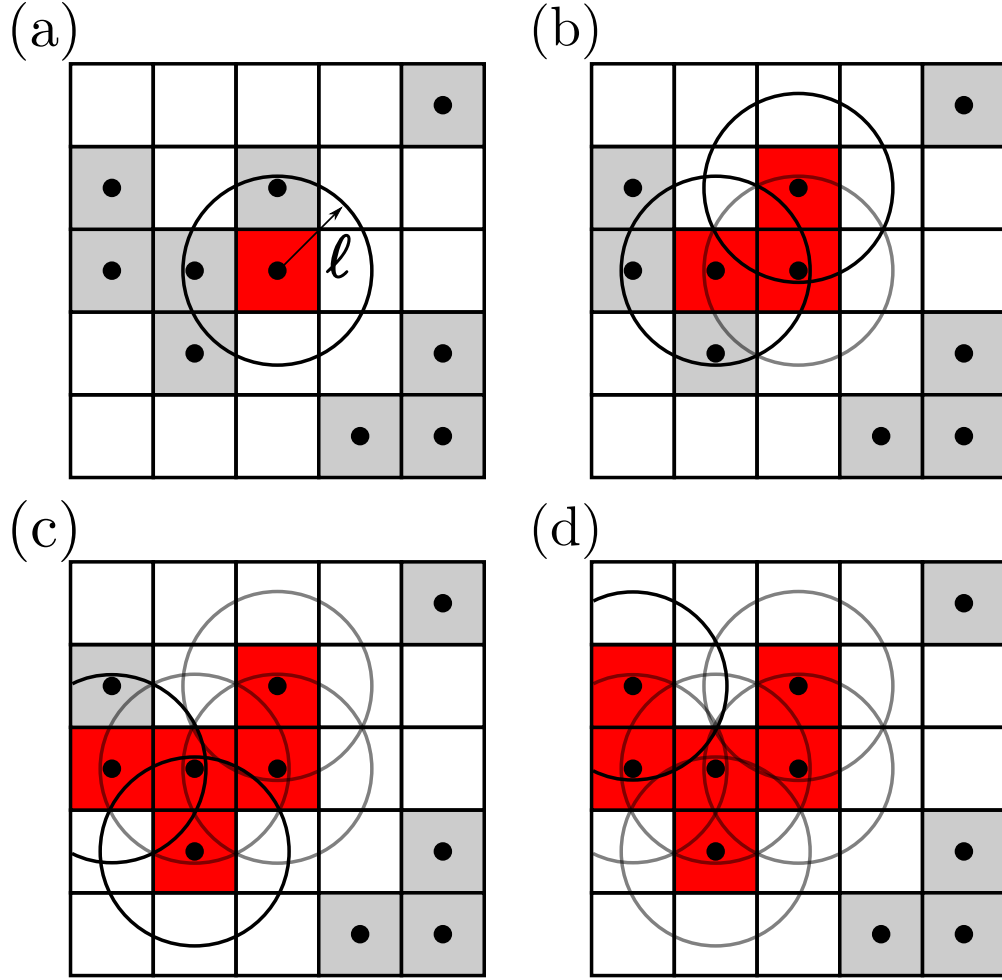


FIG. 2. **The CCA steps (on colors).** The grey and the the red cells are populated ( $D_i > D^*$ ). The small black circles are the geometric centers of each populated cell. The red cells belong the same analyzed cluster. (a) First step: the algorithm select a populated cell and draw a circle of radius  $\ell$ . (b) Second step: the cells with the geometric centers inside the circles of radius  $\ell$  become a part of the red cluster and from their geometric center are drawn others two circles of radius  $\ell$ . The circle of the first step is showed in opaque black. (c) Third step: two more cells became part of the red cluster and two more circles are drawn. (d) Fourth step: the last cell became part of the red cluster. The entire cluster is determined and the algorithm will start to analyze another cluster.

the US cities,

$$\log(\text{AREA}) = a + \alpha_{CCA} \log(\text{POP}), \quad (5)$$

$$\log(\text{NTL}) = b + \beta_{CCA} \log(\text{POP}). \quad (6)$$

The exponents  $\alpha_{CCA}$  and  $\beta_{CCA}$  are obtained through Ordinary Least Square (OLS) [28] fitting to the data for different values of the parameters  $D^*$  and  $\ell$ . The ranges of compatibility and the consistency of the CCA technique are investigated in Figs. 3a-d.

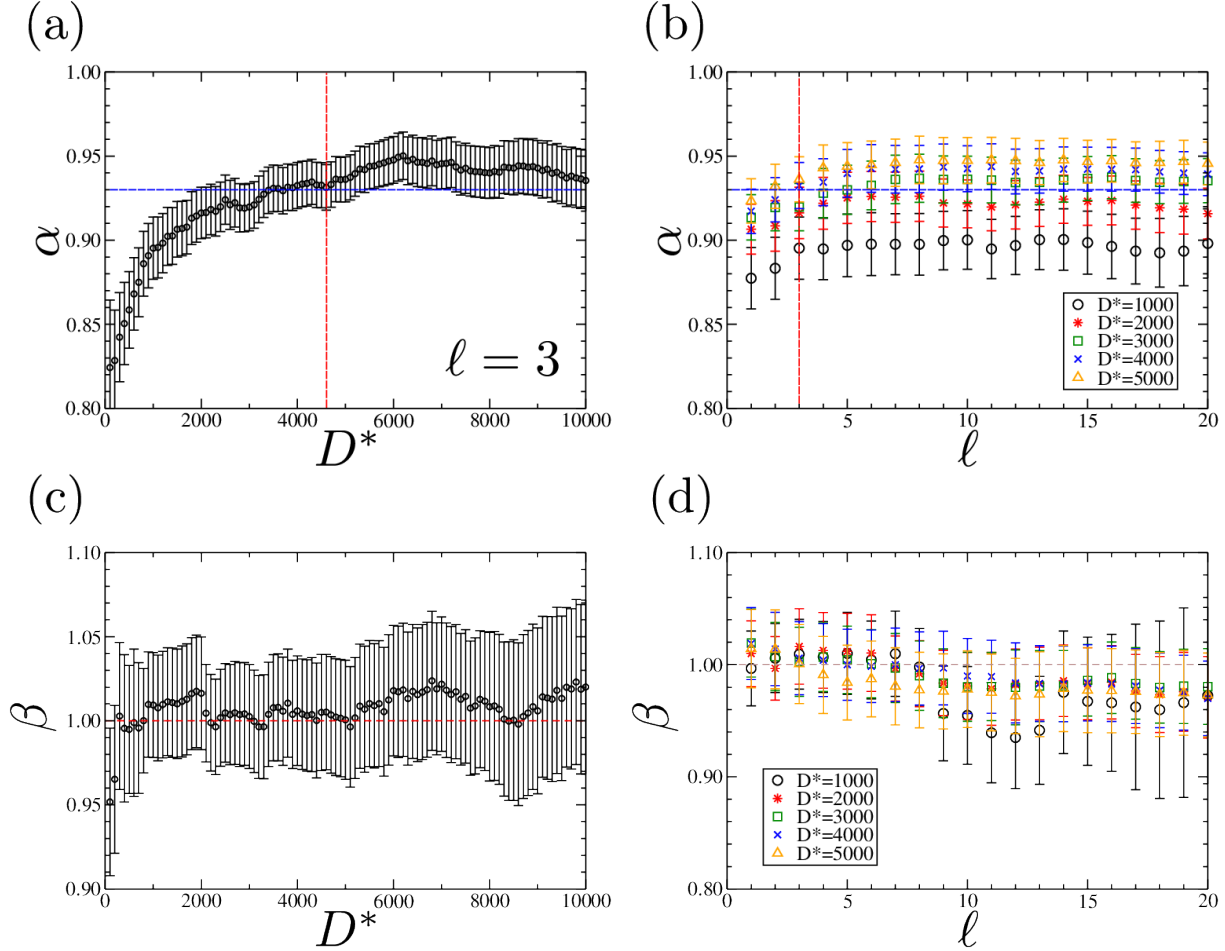


FIG. 3. Allometric exponent  $\alpha_{CCA}$  and  $\beta_{CCA}$  as a function of the parameter  $D^*$  and  $\ell$  (on colors). (a) The exponent  $\alpha_{CCA}$  as a function of  $D^*$  for  $\ell = 3$  km. The parameter  $D^*$  varies from 0 to 10000 *people/km<sup>2</sup>*. For  $D^* > 4000$  and  $\ell = 3$  the allometric exponent  $\alpha_{CCA}$  is between 0.93 (dashed blue line) and 0.95. For  $D^* = 4560$  *people/km<sup>2</sup>* (dashed red line) we observe the arising of five large cities in US Northeast Coast. (b) The exponent  $\alpha_{CCA}$  as a function of the CCA parameter  $\ell$  for  $D^* = 1000, 2000, 3000, 4000,$  and  $5000$  *people/km<sup>2</sup>*. We find a plateau region after  $\ell = 3$  km, where  $\alpha_{CCA} \approx 0.93$  (dashed blue line). (c) The figure shows the allometric exponent  $\beta_{CCA}$  as a function of  $D^*$  for  $\ell = 3$  km. The parameter  $D^*$  varies from 0 to 10000 *people/km<sup>2</sup>*. The dashed red line corresponds to  $\beta = 1$ . (d) The figure shows the allometric exponent  $\beta_{CCA}$  as a function of the CCA parameter  $\ell$  for  $D^* = 1000, 2000, 3000, 4000,$  and  $5000$  *people/km<sup>2</sup>*. The dashed brown line corresponds to  $\beta = 1$ .

Indeed, the definition of the parameters  $D^*$  and  $\ell$  of the CCA affects the dimension and the geometry of the cities, but from the Figs. 3c and 3d, it can be seen that it does not affect the allometric exponent  $\beta_{CCA}$ . Here, our starting strategy is to determine a range of parameters  $D^*$  and  $\ell$  for which the relation between area and population is isometric [15, 17, 19, 20]. We find that for  $D^* > 4000$  and  $\ell = 3$  the allometric exponent  $\alpha_{CCA}$  is between 0.93 and 0.95 and we consider this relation approximately linear. Inside this range, we analyze the result of the CCA using  $D^* = 4560$  and  $\ell = 3$ , where the five larger cities in the US Northeast Coast naturally emerge, as depicted in Fig. 4. We believe that, the lack of an exactly linearity, also inside this range, is due to the high density of some downtowns, specifically, of the most populated urban centers of the US Northeast Coast.

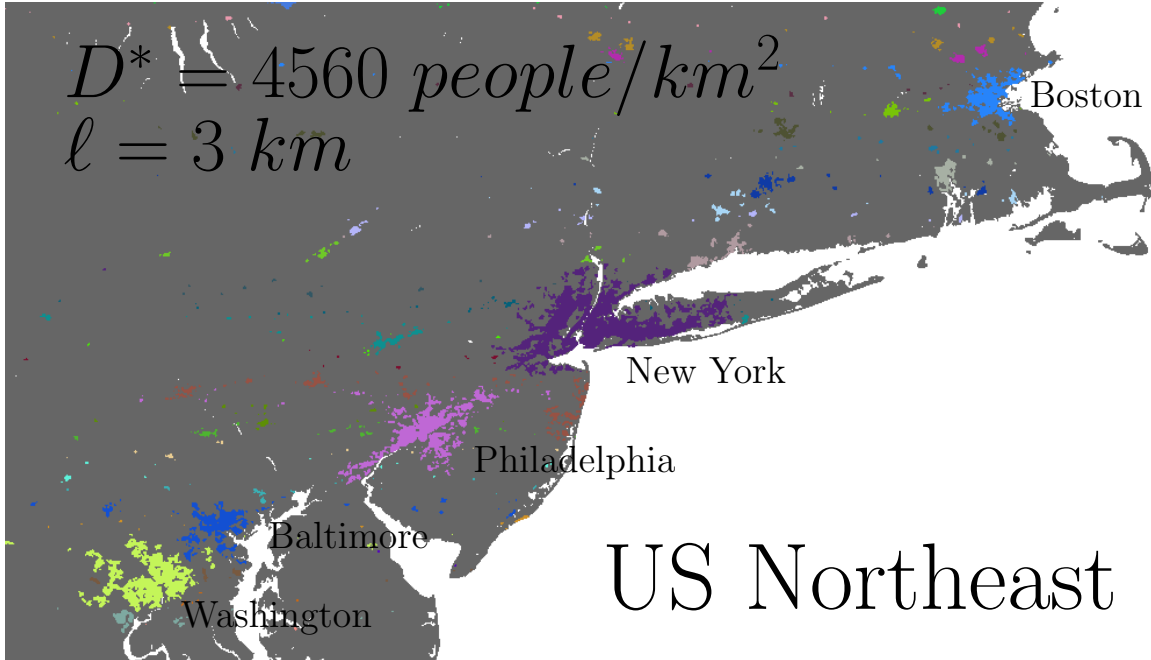


FIG. 4. **Application of CCA to the US Northeast region (on colors).** We use the CCA parameters  $D^* = 4560 \text{ people}/\text{km}^2$  and  $\ell = 3 \text{ km}$ . The clusters of different colors identify different urban agglomerations. Essentially, we distinguish five famous cities such as Boston (light blue), New York (purple), Philadelphia (pink), Baltimore (blue), and Washington D.C. (light green).

For the pair of parameters,  $D^* = 4560$  and  $\ell = 3$ , we find a allometric exponent  $\alpha_{CCA} = 0.93 \pm 0.01$  (Figs. 5a) and a linear scaling between NTL and the population with exponent  $\beta_{CCA} = 1.01 \pm 0.02$  (Figure 6a). Alternatively, others parameters inside this range could be analyzed



without affecting the allometric exponent  $\beta_{CCA}$  (as shown in Figs. 3c and 3d).

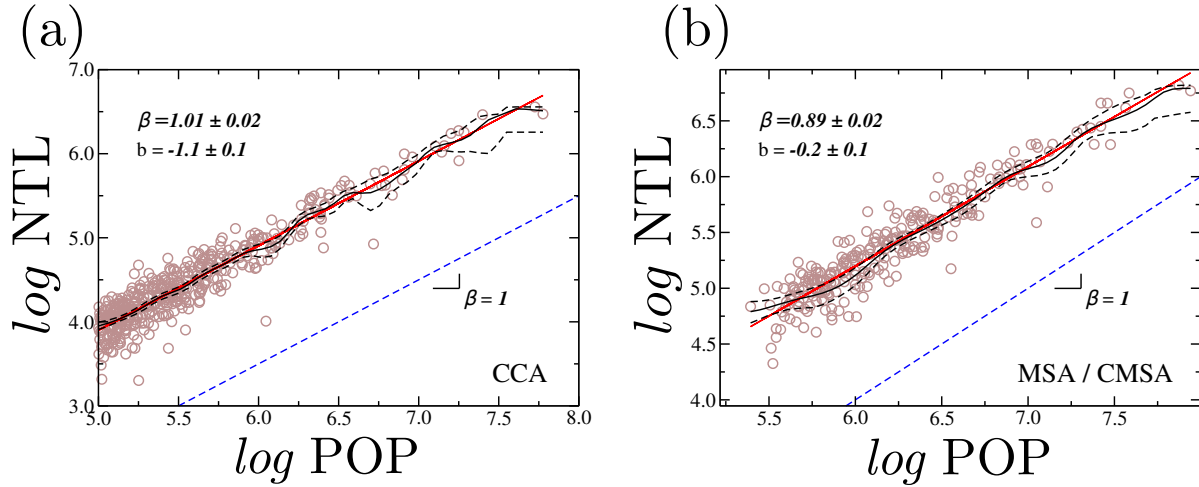


FIG. 5. Allometric exponent  $\alpha$  applying the CCA and using the MSA/CMSA definitions (on colors). (a) The figure shows the allometric scaling law in Eq. 5 and its allometric scaling exponent  $\alpha_{CCA} = 0.93 \pm 0.01$  using CCA parameters  $D^* = 4560 \text{ people/km}^2$  and  $l = 3 \text{ km}$ . The red line is the OLS result, and the solid black line is the N-W estimator. The dashed black lines show the 95% confidence bands of the N-W. The dashed blue line corresponds to  $\alpha = 1$ . (b) The figure shows the allometric scaling exponent  $\alpha_{MSA/CMSA} = 0.49 \pm 0.03$  using the MSA/CMSA definitions. The red line is the OLS result, and the solid black line is the N-W estimator. The dashed black lines show the 95% confidence bands of the N-W. The dashed blue line corresponds to  $\alpha = 1$ .

By analyzing the allometric scaling of the NTL with the population of the US cities using the MSA/CMSA (Fig. 6b), we obtain the allometric exponent  $\beta_{MSA/CMSA} = 0.89 \pm 0.02$ . Such an exponent characterizes a sublinear relation between the NTL and the population, in contrast with the CCA result.

As shown in Fig. 5b, the sublinear scaling behavior of the MSA/CMSA areas as a function of their corresponding populations,  $\alpha_{MSA/CMSA} = 0.49 \pm 0.03$ , clearly suggests that this might not be the most adequate definition of a city agglomerate to be adopted in our study.

As indicated by Oliveira *et al.* [15], the arbitrary geopolitical concept behind the MSA/CMSA seems to overestimate the natural limits of urban areas. In order to illustrate this fact, we show in Fig. 7 the MSA/CMSA of the five most populated US regions, namely, New York-Northern New Jersey-Long Island (NY, NJ, CT, PA), Los Angeles-Riverside-Orange County (CA), Chicago-Gary-Kenosha (IL, IN, WI) and Houston-Galveston-Brazoria (TX). The first and second columns

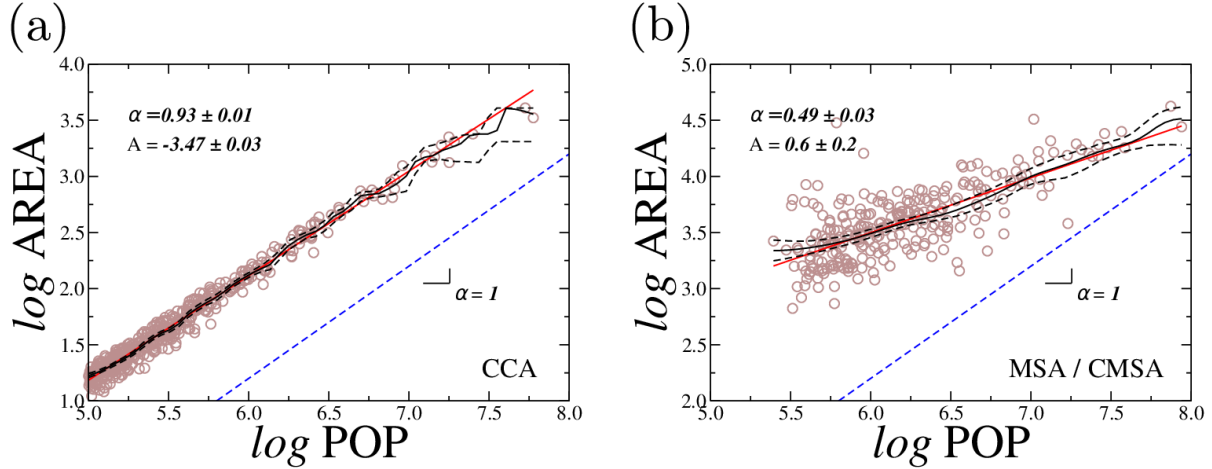
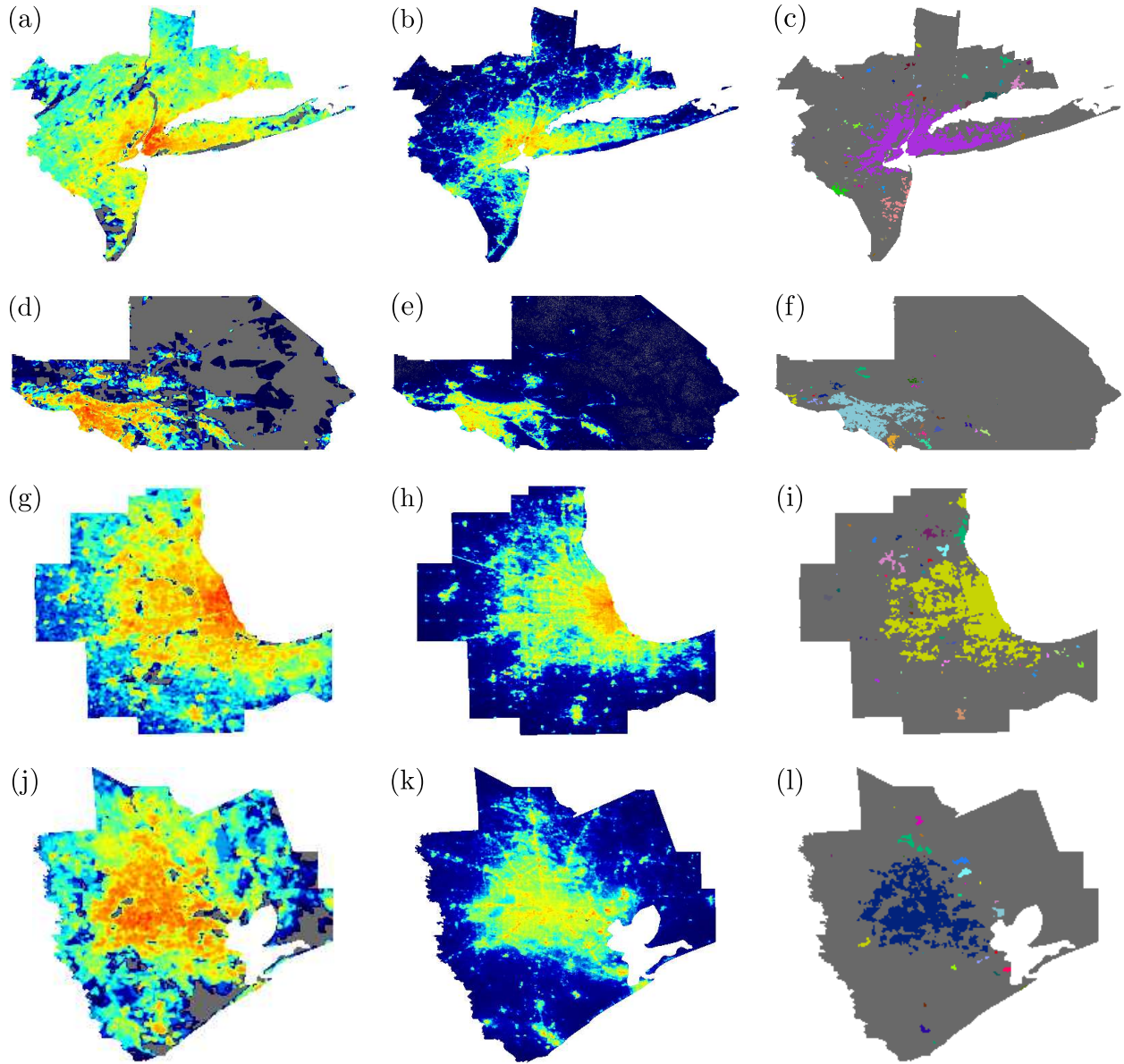


FIG. 6. NTL versus population using the CCA and the MSA/CMSA definitions (on colors). (a) NTL versus population using CCA parameters  $D^* = 4560 \text{ people/km}^2$  and  $l = 3 \text{ km}$ . The graph shows a linear relation between the NTL measured in  $nW/cm^2/sr$  and the population with allometric scaling exponent  $\beta_{CCA} = 1.01 \pm 0.02$  ( $R^2 = 0.88$ ). The solid red line is the linear regression obtained using the OLS method. The solid black line is the N-W estimator and the dashed black lines show the lower and the upper confidence interval (95%)[29, 30]. The dashed blue line corresponds to  $\beta = 1$ . (b) NTL versus population using MSA/CMSA. The graph shows a sublinear relation between the NTL, measured in  $nW/cm^2/sr$ , and the population with allometric scaling exponent  $\beta = 0.89 \pm 0.02$  ( $R^2 = 0.89$ ). The red line is the linear regression and the black line is the N-W estimator. The dashed black lines show the 95% confidence band of the N-W.

show respectively the detailed maps of the population and the NTL datasets. The third column exhibits the cities defined by the CCA with  $D^* = 4560$  and  $\ell = 3$ , as well as the discrepancy between the urban areas belonging to MSA/CMSA and CCA.

## Conclusions

We analyzed the allometric scaling behavior of the NTL as a function of the population of the US cities. Our results corroborate previous works showing that the scaling behaviors of urban indicators with population can be substantially different for distinct definitions of city boundaries. Precisely, using the MSA/CMSA definition, we found a sublinear allometric scaling exponent  $\beta_{MSA/CMSA} = 0.89 \pm 0.02$ . Applying the CCA, we found an exponent  $\beta_{CCA} = 1.01 \pm 0.02$  which indicates an isometric relation between the light pollution and the population of the US urban agglomerations, in clear contrast with the exponent obtained using the MSA/CMSA. Considering



**FIG. 7. Comparison between the CCA and MSA/CMSA (on colors).** Figures (a), (d), (g) and (j) are the human population grid in logarithmic scale obtained from the GPWv4 for the year 2015[22, 23]. Figures (b), (e), (h) and (k) are the NTL measured in logarithmic scale with units  $nW/cm^2/sr$  obtained through the night-time light radiance emission data from the VIIRS DNB[24–26]. In figures (c), (f), (i) and (l) we show the CCA clusters obtained using the CCA parameters  $D^* = 4560 \text{ people}/km^2$  and  $l = 3 \text{ km}$  of the CMSA of: New York-Northern New Jersey-Long Island (NY, NJ, CT, PA), Los Angeles-Riverside-Orange County (CA), Chicago-Gary-Kenosha (IL,IN,WI) and Houston-Galveston-Brazoria (TX). The figures show the discrepancy between the area estimated by the MSA/CMSA and the area delimited by the CCA.

the consistency of the CCA definition in terms of the extensivity between land population and area

of their generated clusters, as demonstrated in previous studies for other urban indicators [15], we come to the conclusion that the proportionality between light pollution and population is indeed correct, as intuitively expected [31]. Under this framework and without loss of generality, it is therefore plausible to utilize NTL as a surrogate for city population in future studies.

The isometric relation between NTL and population of the US urban agglomeration, obtained applying the CCA, imply that small and large cities are proportionally indistinguishable in terms of light pollution. In other words, there is no *economy of scale* or sublinearity concerning the NTL in US cities. Our result shows that a growth of the US cities will aggravate the light pollution and therefore the possible negative effects of the light pollution for the humans and the wildlife health.

## Acknowledgments

We gratefully acknowledge CNPq, CAPES, FUNCAP and the National Institute of Science and Technology for Complex Systems in Brazil for financial support. We especially thank our colleagues and friends H. P. M. Melo and T. A. Amor for the help and the discussions.

## References

- 
- [1] F. Falchi, P. Cinzano, D. Duriscoe, C. C. M. Kyba, C. D. Elvidge, K. Baugh, B. A. Portnov, N. A. Rybnikova, R. Furgoni, The new world atlas of artificial night sky brightness, *Science Advances* 2 (6) (2016) e1600377.
  - [2] N. A. Kerenyi, E. Pandula, G. Feuer, Why the incidence of cancer is increasing: The role of light pollution, *Medical Hypotheses* 33 (2) (1990) 75.
  - [3] D. E. Blask, G. C. Brainard, R. T. Dauchy, J. P. Hanifin, L. K. Davidson, J. A. Krause, L. A. Sauer, M. A. Rivera-Bermudez, M. L. Dubocovich, S. A. Jasser, D. T. Lynch, M. D. Rollag, F. Zalatan, Melatonin-depleted blood from premenopausal women exposed to light at night stimulates growth of human breast cancer xenografts in nude rats, *Cancer Research* 65 (23) (2005) 11174.
  - [4] R. J. Reiter, F. Gultekin, L. C. Manchester, D. Tan, Light pollution, melatonin suppression and cancer growth, *Journal of Pineal Research* 40 (4) (2006) 357.
  - [5] K. J. Navara, R. J. Nelson, The dark side of light at night: Physiological, epidemiological, and ecological consequences, *Journal of Pineal Research* 43 (3) (2007) 215.
  - [6] R. J. Reiter, D. Tan, A. Korkmaz, T. C. Erren, C. Piekarski, H. Tamura, L. C. Manchester, Light at Night, Chronodisruption, Melatonin Suppression, and Cancer Risk: A Review, *Critical Reviews in*

- Oncogenesis 13 (4) (2007) 303.
- [7] R. Chepesiuk, Missing the Dark: Health Effects of Light Pollution, *Environmental Health Perspectives* 117 (1) (2009) A20.
- [8] R. Salgado-Delgado, A. Tapia Osorio, N. Saderi, C. Escobar, Disruption of circadian rhythms: A crucial factor in the etiology of depression, *Depression Research and Treatment* 2011 (839743) (2011) 1.
- [9] M. Aubé, J. Roby, M. Kocifaj, Evaluating Potential Spectral Impacts of Various Artificial Lights on Melatonin Suppression, Photosynthesis, and Star Visibility, *PLoS ONE* 8 (7) (2013) 1.
- [10] United Nations, World's population increasingly urban with more than half living in urban areas, accessed: 2017-06-01 (2014). <http://www.un.org/en/development/desa/news/population/world-urbanization-prospects-2014.html>
- [11] L. M. A. Bettencourt, J. Lobo, D. Helbing, C. Kühnert, G. B. West, Growth, innovation, scaling, and the pace of life in cities, *Proceedings of the National Academy of Sciences of the United States of America* 104 (17) (2007) 7301.
- [12] L. M. A. Bettencourt, G. B. West, A unified theory of urban living, *Nature* 467 (7318) (2010) 912.
- [13] L. M. A. Bettencourt, J. Lobo, D. Strumsky, G. B. West, Urban scaling and its deviations: Revealing the structure of wealth, innovation and crime across cities, *PLoS ONE* 5 (11) (2010) 20.
- [14] H. P. M. Melo, A. A. Moreira, É. Batista, H. A. Makse, J. S. Andrade, Statistical signs of social influence on suicides, *Scientific reports* 4 (6239) (2014) 1.
- [15] E. A. Oliveira, J. S. Andrade, H. A. Makse, Large cities are less green, *Scientific reports* 4 (4235) (2014) 1.
- [16] L. M. A. Bettencourt, J. Lobo, Urban scaling in Europe, *Journal of The Royal Society Interface* 13 (116) (2016) 1.
- [17] C. Caminha, V. Furtado, T. H. C. Pequeno, C. Ponte, H. P. M. Melo, E. A. Oliveira, J. S. Andrade, Human mobility in large cities as a proxy for crime, *PLoS ONE* 12 (2) (2017) e0171609.
- [18] H. A. Makse, S. Havlin, H. E. Stanley, Modelling urban growth patterns, *Nature* 377 (6550) (1995) 608.
- [19] H. D. Rozenfeld, D. Rybski, J. S. Andrade, M. Batty, H. E. Stanley, H. A. Makse, Laws of population growth., *Proceedings of the National Academy of Sciences of the United States of America* 105 (48) (2008) 18702.
- [20] H. D. Rozenfeld, D. Rybski, X. Gabaix, H. A. Makse, The area and population of cities: New insights

- from a different perspective on cities, *American Economic Review* 101 (5) (2011) 2205.
- [21] US Census Bureau, Cartographic Boundary Files, accessed: 2017-06-01 (2014). <http://www.census.gov>
- [22] E. Doxsey-Whitfield, K. MacManus, S. B. Adamo, L. Pistoiesi, J. Squires, O. Borkovska, S. R. Baptista, Taking Advantage of the Improved Availability of Census Data: A First Look at the Gridded Population of the World, Version 4, *Papers in Applied Geography* 1 (3) (2015) 226.
- [23] Socioeconomic data and application center (SEDAC), Gridded Population of the World, Version 4 (GPWv4), accessed: 2017-06-01 (2016). <http://sedac.ciesin.columbia.edu>
- [24] S. Mills, S. Weiss, C. Liang, VIIRS day/night band (DNB) stray light characterization and correction, *SPIE Optical Engineering Applications* 8866 (88661P) (2013) 1.
- [25] National Centers for Environmental Information (NCEI), Visible Infrared Imaging Radiometer Suite (VIIRS), accessed: 2017-06-01 (2016). <http://www.ngdc.noaa.gov/eog/viirs.html>
- [26] National Aeronautics and Space Administration (NASA), Visible Infrared Imaging Radiometer Suite (VIIRS), accessed: 2017-06-01 (2016). <http://npp.gsfc.nasa.gov/viirs.html>
- [27] M. Shimrat, Algorithm 112: Position of point relative to polygon, *Communications of the ACM* 5 (8) (1962) 434.
- [28] D. C. Montgomery, E. A. Peck, G. G. Vining, *Introduction to linear regression analysis*, John Wiley & Sons, 2015.
- [29] E. A. Nadaraya, On estimating regression, *Theory of Probability & Its Applications* 9 (1) (1964) 141.
- [30] G. S. Watson, Smooth regression analysis, *Sankhyā: The Indian Journal of Statistics, Series A* (1964) 359.
- [31] X. Li, X. Wang, J. Zhang, L. Wu, Allometric scaling, size distribution and pattern formation of natural cities, *Palgrave Communications* 1 (15017) (2015) 1.